Talanta 242 (2022) 123286

Contents lists available at ScienceDirect

Talanta

journal homepage: www.elsevier.com/locate/talanta

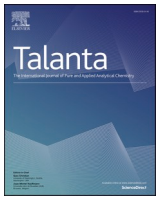

Single-particle inductively coupled plasma mass spectrometry using ammonia reaction gas as a reliable and free-interference determination of metallic nanoparticles

Cristian Suárez-Oubiña, Paloma Herbello-Hermelo, Pilar Bermejo-Barrera, Antonio Moreda-Piñeiro *

Trace Element, Spectroscopy and Speciation Group (GETEE), Institute of Materials iMATUS, Department of Analytical Chemistry, Nutrition and Bromatology. Faculty of Chemistry, Universidade de Santiago de Compostela, Avenida das Ciencias, s/n, 15782, Santiago de Compostela, Spain

ARTICLE INFO

Keywords:
Dynamic-reaction-cell
Single-particle-ICP-MS
Interferences
On-mass approach
Mass-shift approach
Metallic nanoparticles

ABSTRACT

Intensive production of nanomaterials, especially metallic nanoparticles (MNPs), and their release into the environment pose several risks for humans and ecosystem health. Consequently, high-efficiency analytical methodologies are required for control and characterization of these emerging pollutants. Single-particle inductively coupled plasma – mass spectrometry (SP-ICP-MS) is a promising technique which allows the determination and characterization of MNPs. However, several elements or isotopes are hampered by spectral interferences, and dynamic-reaction cell (DRC) technology is becoming a useful tool for free interference determination by ICP-MS. DRC-based SP-ICP-MS methods using ammonia as a reaction gas (either on-mass approach or mass-shift approaches) have been developed for determining titanium dioxide nanoparticles (TiO_2 NPs), copper oxide nanoparticles (CuO NPs), copper nanoparticles (Cu NPs), and zinc oxide nanoparticles (ZnO NPs). The effects of parameters such as ammonia flow rate and dwell time on the peak width (NP transient signal in SP-ICP-MS) were comprehensively studied. Influence of NP size and nature were also investigated.

1. Introduction

A wide variety of nanomaterials (NMs), metallic nanoparticles (NPs) included, are playing an increasing role in medicine and in many industrial sectors such as construction, cosmetics and food [1–5]. The interest in these nanometer-scale materials is due to their unique properties, which differ from those of the chemically identical bulk materials. Moreover, the outstanding properties of NMs are highly dependent on the NM nature and size distribution [6,7]. The increasing use of NMs, and hence their release into the environment and the potential risk to humans and ecosystem health, concerns the scientific community. Several governmental regulatory agencies have brought about regulations such as those in the cosmetic and food industries [8–10]. Undoubtedly, the development and use of NMs must be sustainable, and analytical methodologies are required for an accurate determination/characterization and monitoring.

The determination and characterization of NPs, mainly in complex matrices, is a difficult task, and most common analytical techniques do not provide enough selectivity and sensitivity. In addition, a complete characterization of NPs requires the assessment of several physical-chemical properties, such as surface porosity and functionality, besides the nature (chemical composition), number of NPs and size distribution. In addition to the well-established transmission and scanning electron microscopy (TEM and SEM) and separation techniques, mainly based on flow field fractionation (FFF), inductively coupled plasma mass spectrometry (ICP-MS) in time resolved analysis mode, referred to as single particle ICP-MS (SP-ICPMS), has gained popularity for metallic NPs detection and characterization [11–15]. SP-ICP-MS is able to provide information about the nanoparticle number concentration, size, and number size distribution by monitoring a mass-to-charge ratio of a certain metal contained in the nanoparticle. Moreover, dissolved and particulate analytes can be properly distinguished by measuring the discrete particles (pulses) over a continuous background (dissolved species). The number of particle events is proportional to the particle number concentration in the suspension; whereas, the intensity of each event is proportional to the mass of element per particle. The great counting and sizing capabilities at very low concentrations makes SP-ICP-MS an appealing technique for the assessment of metallic

* Corresponding author.
E-mail address: antonio.moreda@usc.es (A. Moreda-Piñeiro).

https://doi.org/10.1016/j.talanta.2022.123286
Received 22 November 2021; Received in revised form 1 February 2022; Accepted 2 February 2022
Available online 4 February 2022
0039-9140/© 2022 The Authors. Published by Elsevier B.V. This is an open access article under the CC BY license (http://creativecommons.org/licenses/by/4.0/).

nanoparticles (MNPs) in biological and environmental samples [12,13]. However, SP-ICP-MS measurements assume that all measured NPs exhibit a spherical shape, which is not always true when coping with MNPs in environmental, food and clinical matrices. In addition, SP-ICP-MS requires improvements for measuring small MNP sizes [12, 15].

There are several analytes (elements or isotopes) in which determination by ICP-MS is hampered by spectral interferences caused by isobaric isotopes or polyatomic species. These interferences can be overcome by selecting other free-interference isotopes (if available) or by using mathematical corrections against the interfering species. In addition, interference avoidance can be also achieved by improved mass analysers, such as sector field ICP-MS (SF-ICP-MS), and successful applications have been reported for ICP-MS measurements [16–20]. Spectral interferences in ICP-MS can also be overcome by using a quadrupole (a cell) in which the polyatomic interferences collide with a collision gas (typically He in combination with kinetic energy discrimination, KED) or react with a reaction gas such as H_2, NH_3 and O_2 (dynamic reaction cell, DRC). The use of KED and DRC technologies must be properly optimized for removing spectral interferences in SP-ICP-MS, a task which is not as straightforward as in ICP-MS since potential additional interferences can be derived from pollutants, impurities or colloid stabilizers included in the NPs.

Since SP-ICP-MS is an emerging technique for NPs assessment, there are not many applications of DRC technology for interferences removal. The NPs behaviour in the cell is quite different from those exhibited by dissolved analytes. DRC technology leads to ion burst enhancement in the cell, and the ion burst from MNPs is much larger than that observed for dissolved analytes. The experimental evidence leads to the need for lower reaction gas (ammonia) flow rates for MNPs than for dissolved metallic ions [21].

In addition to the reaction gas flow rate, ICP-MS instrumentation with quadrupole ion deflector requires the careful optimization of the Mathieu or Rejection Parameters (RPa and RPq) in the reaction cell, parameters which correspond to the high-mass and low-mass cut-off, respectively. Moreover, NPs determination by SP-ICP-MS with DRC requires the evaluation of the effect of the dwell time and the width peak on the number of particle and particle size in order to avoid under- or over-estimations. Research literatures mention the use of O_2 for SP-ICP-MS assessment of SiO_2 NPs [22], TiO_2 NPs [23], and Au, Ag, Pt and Fe_3O_4 NPs [24]. In addition, studies based on the use of H_2, NH_3 and CH_3F as reaction gases for SiO_2 NPs determination [22], H_2 for Au, Ag, Pt and Fe_3O_4 NPs [24], and NH_3 for SP-ICP-MS determination of TiO_2 NPs [25], have also been reported. High reactivity, and hence high sensitivity, and the generation of predictable adducts (mass shift approach), has been reported for O_2; whereas, H_2 has been found useful for overcoming Ar interferences [22,25]. However, an unpredictable reactivity has been reported for NH_3 and CH_3F reaction gases, offering the advantage of generating several adducts or ion-products, and hence higher selectivity in ICP-MS/MS for interferences removal by using either on-mass and mass-shift approaches [26,27].

As previously commented, literature regarding DRC technology for spectral interferences removal is mainly focused on conventional ICP-MS [21], although there are some developments for sedimentation field-flow fractionation (SdFFF) coupled to ICP-MS/MS [28] and more recently for SP-ICP-MS [22–25]. The aim of the current research has been to test the feasibility of DRC-SP-ICP-MS using NH_3 as a reaction gas for a free-interference determination of TiO_2 NPs, Cu NPs, CuO NPs, and ZnO NPs. In addition to the NPs' nature (chemical composition), the effect of the NPs size, as well as the dwell time and NH_3 flow rate, was also investigated in on-mass and mass-shift measurement modes. Findings from this research will be useful to improve the use of reaction gases in SP-ICP-MS analysis and the application to challenging complex matrix analysis.

2. Experimental

2.1. Instrumentation

A NexION 2000 inductively coupled plasma mass spectrometer (PerkinElmer, Waltham, MA, USA) equipped with dynamic reaction cell (DRC) technology and Single Cell Micro DX autosampler (PerkinElmer) was used for determinations. The instrument is equipped with nickel sampler/skimmer/hyper skimmer cones. The nebulizer was a concentric Meinhard™ type coupled to a cyclonic spray chamber (Glass Expansion, Inc., Melbourne, Australia) and attached to a quartz torch with a quartz injector tube (2.5 mm i.d.). Data acquisition and management was performed with the Syngistix™ Nano Application 2.5 version software (PerkinElmer), which allows data visualization as it is being acquired in real-time and displays background-corrected intensity histogram which continuously updates during data acquisition [29]. The software uses the same formula regarding the basic principles of SP-ICP-MS [12] for assessing the number of NPs and NPs sizes. An USC-TH ultrasound water bath (45 Hz, 80 W) from VWR International Eurolab S.L (Barcelona, Spain) was used for dispersing NPs before analysis.

2.2. Reagents and standards

All solutions were prepared with ultrapure water (18.2 MΩ cm of resistivity) obtained from a Milli-Q® IQ 7003 purification device system (Millipore, Bedford, MA, USA). Mono-elemental 1000 mg L^{-1}standards of titanium [$(NH_4)_2TiF_6$] and copper [$Cu(NO_3)_2$] were purchased from PerkinElmer; whereas, mono-elemental standard of zinc [$Zn(NO_3)_2$] was from Merck (Darmstadt, Germany). Gold NPs solutions were prepared from a N8151035 (49.6 nm by TEM, 12.4 ng mL^{-1}, 9.89 × 10^6 NPs mL^{-1}, in aqueous 1 mM citrate) certified reference material from nano Composix (San Diego, CA, USA). Titanium dioxide nanoparticles stock suspensions (100 mg L^{-1} as TiO_2 in ultrapure water) were prepared from TiO_2 nanopowder (rutile, 99.9%) of 30, 50 and 100 nm aerodynamic particle size (APS) purchased from US Research Nanomaterials (Houston, TX, USA), and TiO_2 suspension (mixture of rutile and anatase, 99.5%, size <150 nm, 40 wt % in water) purchased from Sigma-Aldrich. Zinc oxide NPs suspensions (100 mg L^{-1} as ZnO in ultrapure water) were prepared from 35 to 45 and 80–200 nm ZnO nanopowder from US Research Nanomaterials, and ZnO dispersion (size <100 nm, 20 wt % in water) purchased from Sigma-Aldrich. Copper NPs suspensions were prepared from 40 to 60 and 60–80 nm Cu nanopowder (99.5%) and Cu O nanopowder (size <50 nm) from Sigma-Aldrich (stock suspensions at 100 mg L^{-1} as Cu and CuO in ultrapure water, respectively). Stock suspensions, as well as further diluted suspension were prepared without adding stabilizing agents and homogenization before sampling was performed by ultrasound stirring (except for Au NPs). NexION Setup Solution, 10 μg L^{-1}Be, In, U, and Ce, was from PerkinElmer. Hyperpure nitric acid 69% (w/v) was from Panreac (Barcelona, Spain). Argon (99.998%) and ammonia (99,999%) were from Nippon Gases (Madrid, Spain).

Glassware and plastic ware was decontaminated by soaking in 10% (v/v) nitric acid for at least 48 h. The material was then rinsed with ultra–pure water several times.

2.3. SP-ICP-MS measurements

SP-ICP-MS settings are listed in Table 1. Since an exact mass-to-charge ratio is not isolated with the quadrupole ion deflector (axial field voltage, AFT at 350 V), RPa (high-mass cut-off) and RPq (low-mass cut-off) rejection parameters have to be fixed at the optimum values for a better focusing of the mass-to-charge ratio of interest (adduct in mass shift approach, and the analyte in on-mass approach). RPa was found to be less significant for both on-mass and mass shift approaches, and this parameter was fixed at 0 for all NPs and both measurement modes. However, RPq was found to be quite important [21], and the optimized

Table 1
Operating conditions for SP-ICP-MS measurements.

Parameter (units)	
Instrument	Nex Ion 2000
Spray chamber	QuartzCyclonic
PC^{3x} Peltier Cooler System	4 ℃
Nebulizer type	Concentric Meinhard™
RF power (W)	1600
Plasma gas flow rate (L min^{-1})	15
Auxiliary gas flow rate (L min^{-1})	1.2
Nebulizer gas flow rate (L min^{-1})	1.14
Sample flow rate (mL min^{-1})	≈0.21
Quadrupole ion deflector (V)	Set for maximum ion transmission
Transport efficiency (%)	≈8%
Scan time (s)	100

values for on-mass and mass shift measurement modes are displayed in Table 2.

Daily performance was assessed by monitoring Be, In, U, Ce (Ce++/Ce and CeO/Ce ratios) and background (mass-to-charge ratio of 202), and verifying intensities higher than the values established as optimum by the manufacturer. Transport efficiency (TE%) was assessed by the particle frequency method, which implies the assessment of the sample flow rate, an aqueous ionic Au calibration, and the measurement of an Au NPs certified reference material. Therefore, sample flow rate was established by aspirating ultrapure water and weighing the solution after and before aspiration at the selected pump conditions (sample flow rates were between 0.19 and 0.21 mL min^{-1}). Ionic Au calibration was performed within the 0–3.5 μg L^{-1} range, and a suspension at 1.0×10^5 particles mL^{-1}, prepared in ultrapure water from a 49.6 nm Au NPs certified reference material, was finally measured. Transport efficiency (TE%) values (close to 8.0%) were automatically calculated by Syngistix™ Nano Application.

Matched 1.0% (v/v) nitric acid calibrations covering ionic Ti, Zn, and Cu concentrations within the 0.1–10 μg L^{-1} range (five level concentrations) were prepared for the assessment of NPs size distribution [11]). Reagent blanks (1.0% (v/v) nitric acid) were also analysed throughout the work.

Stock NPs suspensions were properly diluted in ultrapure water and sonicated just before SP-ICP-MS measurements to avoid agglomeration and aggregation phenomena. NPs standards concentrations varied from 0.5 to 5.0 μg L^{-1} depending on the analyte and mainly on the measurement mode. Therefore, the standard mode and the on-mass approach require similar concentrations for achieving an adequate number of peaks in the time window detection of 100 s and size distribution close to a Gaussian distribution. However, mass-shift measurements require higher concentrations.

Table 2
Optimized SP-ICP-MS conditions for mass-shift and on-mass approaches.

Analyte	Monitored ion/adduct	Monitored *m/z*	Mode	NH_3 flow rate (mL min^{-1})	Dwell time (μs)	RPq
Ti	$Ti(NH)(NH_3)_3$	114	Mass-shift	0.5–0.75	100	0.2
	$Ti(NH)(NH_3)_4$	131	Mass-shift	0.75–1.0	100	0.2
Cu	Cu	63	On-mass	0.5	50	0.5
	$Cu(NH_3)_2$	97	Mass-shift	1.25	100	0.2
Zn	Zn	64	On-mass	0.25	50	0.35
	$Zn(NH_3)_3$	115	Mass-shift	1.75	200	0.2

2.4. Data treatment

Origin8 Pro software (OriginLab Corporation, Northampton, MA, USA) was used for peak integration. Raw data from Syngistix ICP-MS software (1.0 million measurements) were first exported to Excel and treated (filtered) to remove low intense peaks (few cps, as well as 0 cps) and reduced the data set. Filtered data were then exported to Origin8 for peak integration by a semi-automatic procedure. First, the baseline was established by fixing the area without peaks and then the peaks were selected for automatic integration by the software. At least 10 peaks were integrated to assess mean peak widths under each condition, and the selected peaks were those of intermediate height (intensity) for avoiding the selection of peaks located in the wings of the distribution. Integration was carried out and the peak width at the baseline (whole peak) and at different heights (5, 15 and 50% of peak height) was obtained. The data generated was manually checked and listed, and, the mean and the standard deviation of peak widths after integration were calculated for interpretation and/or plotting.

3. Results and discussion

The effect of the ammonia flow rate, dwell time and work-modes using ammonia as a reaction gas have been evaluated for both on-mass and mass-shift approaches, and compared with vented mode in each specific conditions. In addition, the effect of these experimental parameters on peak shape, peak intensity, and peak stability was also evaluated by measuring the peak width at different heights (baseline, 5%, 15% and 50%). The studies were focused on TiO_2 NPs, Cu NPs, CuO NPs, and ZnO NPs of several size distributions.

3.1. Selection of the ammonia-based adducts

After fixing optimum RPq Mathieu parameter and ammonia flow rate [21], mass scanning experiments were performed to obtain the several ammonia ion products for each element using ionic Ti, Cu, and Zn standards at 5 μg L^{-1} (solutions prepared in 1.0%(v/v) nitric acid) and the ICP-MS operating conditions listed in Table 1. The most intense signals for Ti were observed at *m/z* ratios of 63, 114 and 131, which correspond to $^{48}Ti(NH)$, $Ti(NH)(NH_3)_3$ and $Ti(NH)(NH_3)_4$ clusters, respectively (Fig. 1A). Other intense signals have been observed for *m/z* 49 and 46 (Fig. 1A), but they do not come from Ti (lack of Ti isotopic pattern in the signals). It has been reported in the literature that $^{48}Ti(NH_3)_6$ (*m/z* 150) is a suitable ammonia ion product for Ti assessment by ICP-MS [26,30,31] and SdFFF-ICP-MS/MS [28]. Other reported ammonia-based adducts for Ti have been $^{48}TiNH_2(NH_3)_4^+$(*m/z* 132) in ICP-MS measurements [32], and $^{48}Ti(NH)$ (*m/z* 63) in SP-ICP-MS analysis [25]. The *m/z* 114 and 131 have been finally selected for further mass shift studies. However, *m/z* 63 was not further used since the NexIon 2000 is equipped with a quadrupole ion deflector which is not a real quadrupole, and low *m/z* ratios could be not excluded and be present in the reaction cell (^{63}Cu and ^{63}Zn could be potential interferences).

Fig. 1B and C shows the mass spectra for Cu (ammonium flow rate of 1.5 mL min^{-1}) and Zn (ammonium flow rate of 2.0 mL min^{-1}), respectively (RPq of 0.20). The highest signals were obtained at *m/z* ratios of 97 and 115 for Cu and Zn, respectively, which correspond to $^{63}Cu(NH_3)_2^+$ and $^{64}Zn(NH_3)_3^+$ ion products (mass shift approach). Findings regarding Cu agree with those obtained by Fu et al. [32] when using an ammonia/helium mixture for DRC-ICP-MS. However, the *m/z* 115 adduct for Zn is different from that previously proposed (*m/z* of 100, $^{66}Zn(NH_3)_2^+$) [32]. Other comparisons were not possible because, although ammonia has been used as a reaction gas in DRC-ICP-MS, the measurement methods were based on on-mass approaches [33–37]. It must be noted that the formation of adducts from the *m/z* of interest is less efficient when using ammonia as a reaction gas than when using other reaction gases such as oxygen and hydrogen [26]. However, ammonia as a reaction gas is appealing in DRC because the high

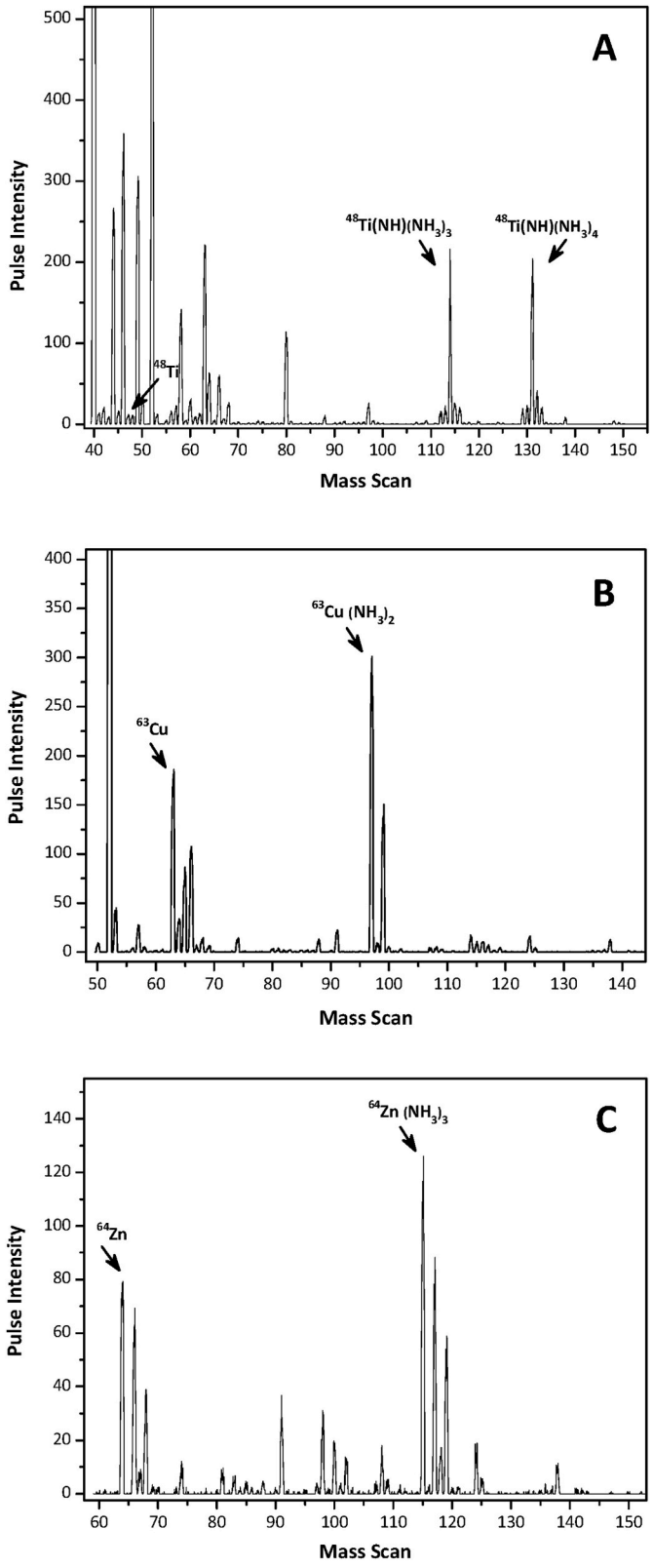

Fig. 1. Mass spectra illustrating adducts that are formed with ammonia: (A) Ti, 1.0 mL min^{-1}, (B) Cu, 1.5 mL min^{-1} and (C) Zn, 2.0 mL min^{-1}.

selectivity achieved (adducts of high *m/z* ratios are formed and mass shift measurements can be carry out at a large and free-interference region of the mass spectra).

3.2. Effect of ammonia flow rate

The effect of ammonia flow rate (mass shift and on-mass measurements) has been studied for TiO_2, Cu, CuO, and ZnO NPs of several size distributions. The effect on the formation of metal-ammonia adducts (mass shift approach) was performed for TiO_2, Cu, and CuO NPs; whereas, the on-mass approach was focused on the specific elemental masses ^{63}Cu and ^{64}Zn. On-mass measurements for Ti and mass shift measurements for Zn were not performed due to the low sensitivity and/or inefficient formation of ammonia-based adducts. The axial field voltage (AFT) was set at 350 V (default value) for all measurements. Similarly, the rejection parameter RPa was set at 0 (on mass and mass-shift approaches) for all cases since the influence of this parameter was scarce. Regarding RPq parameter, previous optimized values for each analyte and measurement mode [21] were fixed (Table 2); whereas, the deflector voltage was daily set at the specific element mass to achieve maximum ion transmission in the reaction cell.

Suspensions of TiO_2 NPs of 30, 50 and 100 nm (1.25 μg L^{-1} of TiO_2), and <150 nm (2.5 μg L^{-1} of TiO_2) were analysed under ammonia flow rates within the 0.25–1.0 mL min^{-1}(adduct ^{48}Ti(NH)(NH$_3$)$_3$, *m/z* of 114), and from 0.5 to 1.25 mL min^{-1} when monitoring the ^{48}Ti(NH)(NH$_3$)$_4$ adduct (*m/z* of 131). RPq value was set at 0.20 (Table 2) and measurements were performed with a dwell time of 50 μs for monitoring both ammonia-based adducts. As expected [23,24], broad signals (higher peak width at baseline, and also at 5%, 15% and 50% height) were measured when using reaction gas (ammonia) respect to the vented mode (no reaction gas), and the peak width was found to be increased with higher ammonia flow rates (Fig. 2). For Ti, narrower peaks were obtained when monitoring the ^{48}Ti(NH)(NH$_3$)$_3$ adduct (*m/z* of 114) than those observed for the ^{48}Ti(NH)(NH$_3$)$_4$ adduct (*m/z* of 131), and therefore^{48}Ti(NH)(NH$_3$)$_3$ monitoring appears to be more appealing since the narrow peaks obtained (less tailing). However, since the quadrupole ion deflector in the instrument does not select a specific *m/z* ratio, the adduct of *m/z* of 114 could be interfered from ^{114}Cd, and from other polyatomic adducts formed from the matrix sample such as ^{98}Mo^{16}O, ^{98}Ru^{16}O, and also from products formed with ammonia (^{63}Zn(NH$_3$)$_3$). Therefore, although broader peaks (large tailings) are obtained for ^{48}Ti(NH)(NH$_3$)$_4$, the peak weight is lower than 6.0 ms for all ammonia flow rates (Fig. 2), and this adduct is preferable since the measurement is moved to a region of large *m/z* ratios (*m/z* of 131) which is potentially free of interferences.

From Fig. 2 (peak widths), and also by analysing the number of peaks and peak intensities (Table S1, electronic supplementary information, ESI), and peak shape from raw spectra (Fig. S1 and S2, ESI), the most suited ammonia flow rates were 0.50 and 0.75 mL min^{-1} when monitoring the Ti(NH)(NH$_3$)$_3$ adducts, and higher rates, within the 0.75–1.0 mL min^{-1} range, for Ti(NH)(NH$_3$)$_4$ adduct measurement. Low ammonia flow rate have led to low peak intensities and a low number of peaks recorded, but high ammonia flow rate also reduce the peak intensities as well as the number of peaks because a dilution effect. Therefore, intermediate ammonia flow rates, which exhibit low peak widths, high number of peaks and moderate peak intensities, have been selected for Ti-based ammonia adducts. Comparison with ICP-MS based on DRC with ammonia as a reaction gas led to lower ammonia flow rates in SP-ICP-MS than in ICP-MS. This finding is attributed to the hundreds of atoms inside the NPs which increase the ammonia reactivity in the cell due to a vigorous ion-burst compared to single atoms one-by-one [24].

As shown in Fig. 2 for TiO_2 NPs, and also for other NPs (figures in the ESI section), the NP size have a small influence on the peak width, and broader peaks are not related to TiO_2 NPs of higher sizes (Fig. 2A–C). In the case of TiO_2 NPs <150 nm (Fig. 2D), the narrow peaks must be attributed to a high proportion of TiO_2 NPs of small size in the suspension prepared from this standard (the manufacturer states that the material contains TiO_2 NPs <150 nm). In addition, NPs agglomeration also influences the peak widths since larger ion bursts are produced from the agglomerate than those produced from disperse NPs. Finally, peak

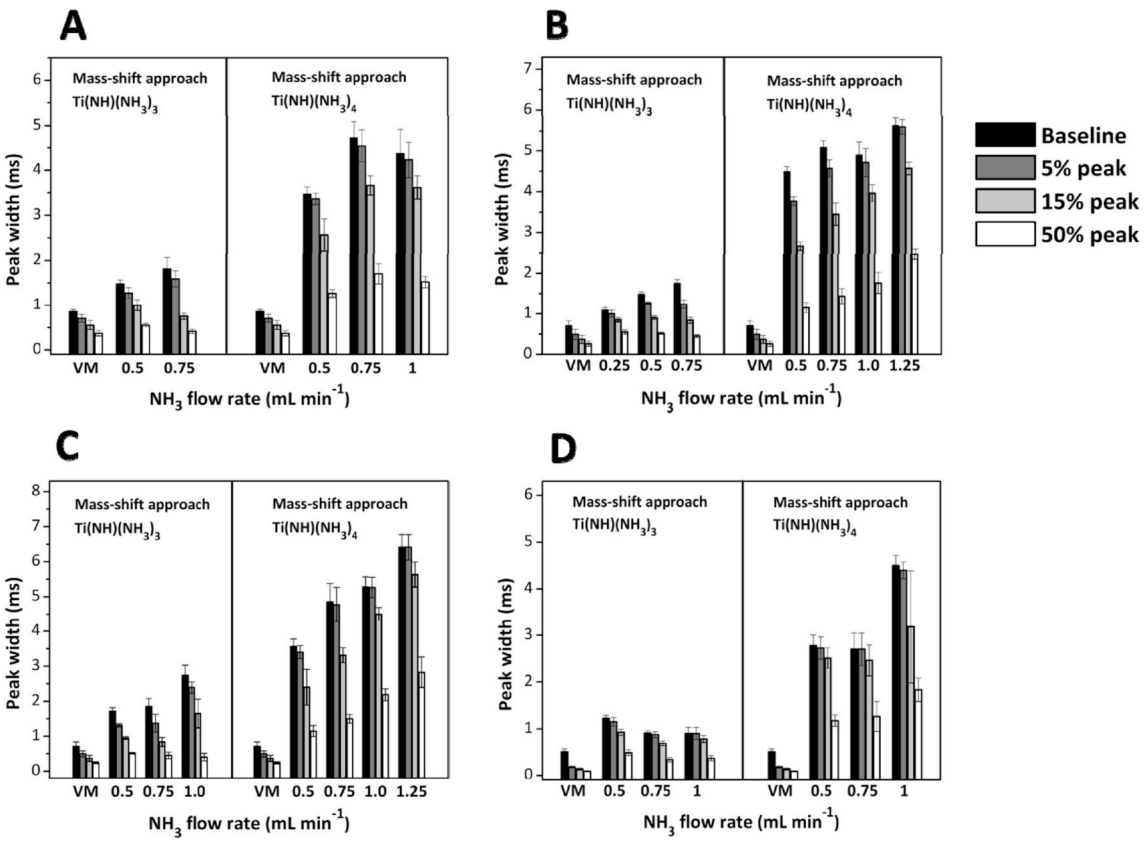

Fig. 2. Effect of the ammonia flow rate on the peak width recorded by using mass-shift approach from TiO_2 NPs of (A) 30 nm, (B) 50 nm, (C) 100 nm, and (D) < 150 nm.

widths are strongly dependent on the ion-product selected (Ti-131 against Ti-114) for the same conditions and NPs size (and also for Cu-63 and Cu-97, and for Zn-64 and Zn-115). Thus, boarder peaks are obtained from to the largest ion-product (Ti-131 against Ti-114).

Regarding Cu and CuO NPs, on-mass and mass-shift approaches using several ammonia flow rates were compared using a dwell time of 50 μs, and RPq values of 0.2 for mass-shift approach and 0.5 for on-mass approach. Suspensions of 40–60 nm and 60–80 nm Cu NPs (2.5 μg L^{-1} of Cu), and <50 nm CuO (2.5 μg L^{-1} of CuO) were tested at flow rates from 0.25 to 0.75 mL min^{-1} and from 0.75 to 2.0 mL min^{-1} for the on-mass approach and mass-shift approach, respectively. Similarly to TiO_2 NPs, results showed a clear correlation between the ammonia flow added and the peak width (Fig. S3, ESI); whereas, "noisy" spectra are observed when ammonia flow was added, especially at 1.5 mL min^{-1}ammonia (mass-shift mode), as shown in Fig. S4 (ESI). Taking into account parameters such as the number of peaks and peak intensities (Table S1, ESI) and peak widths in Fig. S3 (ESI), the most suitable flow rates were 0.4–0.5 mL min^{-1} (on-mass approach) and 1.25–1.5 mL min^{-1}(mass shift mode), slightly lower than those required for Cu determination in ICP-MS with ammonia-based DRC (1.5 mL min^{-1} in previous experiments) [21]. As shown in Fig. S3 (ESI), CuO and Cu NPs measurements based on the on-mass approach were also possible using low ammonia flow rates.

The effect of the ammonia flow rate on ZnO NPs measurements (dwell time of 50 μs and RPq of 0.2) were performed with suspensions of ZnO NPs of 35–45 nm (1.25 μg L^{-1}), 80–200 nm (2.5 μg L^{-1}), and <150 nm (2.5 μg L^{-1}). As shown in Fig. S5B (ESI) the mass shift approach (RPq of 0.2) was only possible when using the ZnO NPs of largest size (80–200 nm), which shows spectra with enough intense peaks for peak height measurement at high ammonia flow rates (1.5–2.25 mL min^{-1}). However, very few and small signals were observed for ZnO NPs standards of lower size distribution (Table S1, ESI), and improvements were not obtained when using the highest ammonia flow rates (dilution effect). These findings are quite similar to those obtained for other NPs, such as Fe_3O_4 NPs [24,37], and a proper measurement of the adducts was reported to require the use of higher dwell times (the effect of the dwell time will be discussed in the following sections). An ammonia flow rate of 1.75 mL min^{-1} when analysing 80–200 nm ZnO NPs was therefore selected for further studies.

Regarding on-mass mode measurement for ZnO NPs (RPq of 0.35), Fig. S5(A-C) and Table S1 (ESI) shows that low ammonia flow rates (from 0.1 to 0.5 mL min^{-1}) allow the measurement of intense ^{64}Zn signals for all ZnO suspensions (low and high sizes), being the number of peak quite constant within the 0.1–0.5 mL min^{-1} ammonia flow rate. On-mass measurement mode seems therefore to be an efficient approach for interferences removal in ZnO NPs assessment. In addition, a dwell time of 50 μs is adequate for ZnO NPs on-mass measurements. An assessment between standard mode and several ammonia flow rates for on-mass approach was performed as well (Fig. S6).

Finally, it must be noted that the mass shift approach with high ammonia flow rate, case of the measurements of $^{48}Ti(NH)(NH_3)_4$ (*m/z* 131) adduct, may have an effect of the NPs size distribution since the broader peaks obtained.

3.3. *Influence of dwell time*

A suitable dwell time must be selected regarding possible multi-peak coincidence, high backgrounds or under/overestimation in NP concentration or size [12,13,36]. Therefore, dwell times of 20, 50, 100 and 200 μs were studied. As an example, Fig. 3 shows TiO_2 NPs peak shapes obtained for low (20 and 50 μs, Fig. 3A and B, respectively), intermediate (100 μs, Fig. 3C), and high (200 μs, Fig. 3D) dwell times. The use of low dwell times gives noisy peaks (Fig. 3A and B), which are attributed to ion-burst with nanoparticles in reaction cell; whereas, measurements

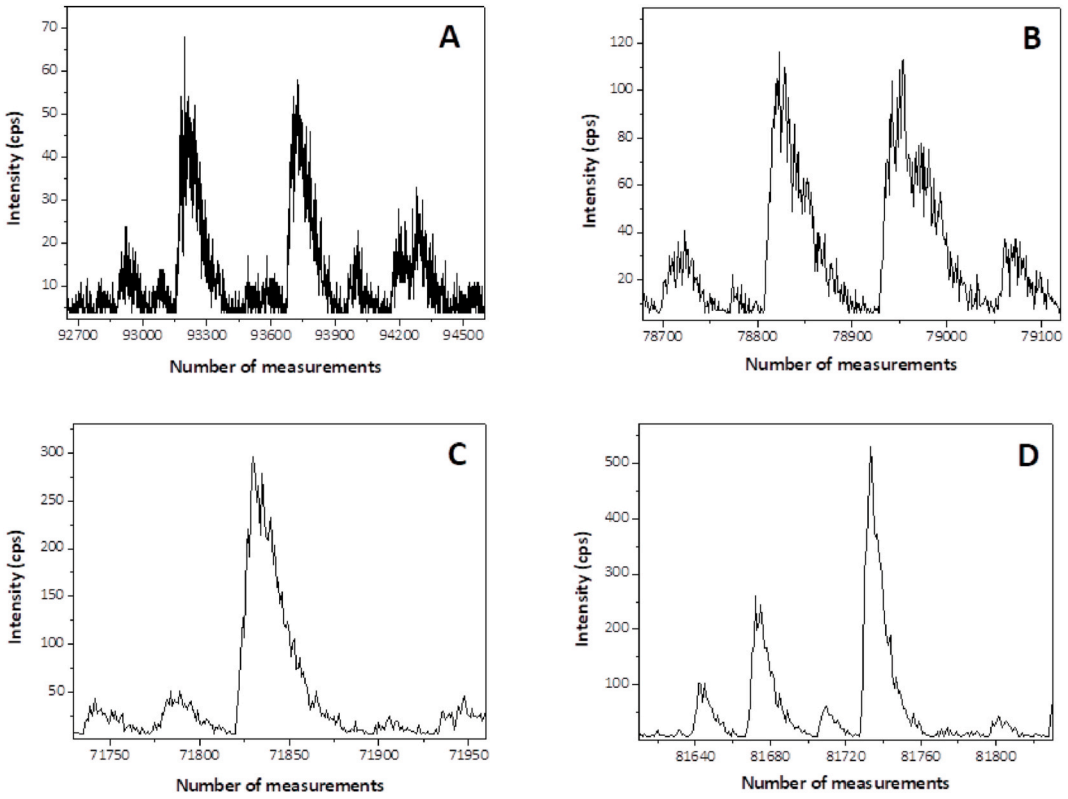

Fig. 3. Raw data peaks obtained from SP-ICP-MS measurements for TiO_2 NPs of 100 nm. (m/z 131) at 1.0 mL min^{-1} ammonia and dwell times of (A) 20 μs, (B) 50 μs, (C) 100 μs, and (D) 200 μs

at 200 μs could lead to multi-peak coincidence probability (broad peaks in Fig. 3D and high intensities and low number of peaks as listed in Table S1, ESI) and hence high background (dissolved analyte) and low particle concentrations (low number of peaks) as listed in Table S1 (ESI). However, a dwell time of 100 μs (Fig. 3C) implies enough time for detection of discrete TiO_2 NPs with several measured points that can define the peaks properly without any fractionation.

The effect of the dwell time on registered peak weight for TiO_2 NPs of several size distributions [suspensions of TiO_2 NPs of 30, 50 and 100 nm (1.25 μg L^{-1} of TiO_2), and <150 nm (2.5 μg L^{-1} of TiO_2)] is shown in Fig. S7 (ESI). This effect was illustrated with TiO_2 NPs of 50 nm registering $^{48}Ti(NH)(NH_3)_4$ ion product as it can be observed in Fig. S8. Ammonia flow rates were fixed at 0.75 mL min^{-1} when recording the $^{48}Ti(NH)(NH_3)_3$ adduct, and 1.0 mL min^{-1} for $^{48}Ti(NH)(NH_3)_4$ measurement. The effect of the dwell time under standard conditions (vented mode) is also shown in Fig. S7 (ESI). In general, the peak width follows a clear correlation with the dwell time, and high dwell times lead to the broadest peaks. However, taking into account the peak shape in the spectra (Fig. 3), as well as the peak widths, the number of peaks and the peak intensities (Table S2, ESI), detected signals with a dwell time of 100 μs seem to be more reliable than peaks recorded with lower dwell times such as 20 and 50 μs Peak fractionation (mainly when using a dwell time of 20 μs) can occur (low peak intensities as listed in Table S2, ESI); whereas, a dwell time of 200 μs led to a lower number of peaks (peak coincidence events) and a higher amount of ionic Ti concentration (Table S2, ESI), obtaining biased measurements.

Experiments for Cu and CuO NPs [suspensions of 40–60 nm and 60–80 nm Cu NPs (2.5 μg L^{-1} of Cu), and <50 nm CuO (2.5 μg L^{-1} of CuO)] were performed by setting an ammonia flow rate of 0.5 mL min^{-1} for on-mass measurements (^{63}Cu) and 1.5 mL min^{-1} when using the mass shift approach ($^{63}Cu(NH_3)_2$). The effect of the dwell time on Cu and CuO NPs peak weights (Fig. 4) was similar to those observed for TiO_2 NPs, and moderate peak weights, as well as a large number of intense peaks (Table S2, ESI), were observed at intermediate dwell times (50 and 100 μs). Large dwell times could lead to multi-peak coincidence (Fig. S9 and S10, ESI) which agrees with the lower number of peaks detected when using a dwell time of 200 μs (Table S2, ESI). Recording at low dwell times such as 50 μs gives adequate (clean) peaks and 50 μs is enough to register well-defined peaks and signal stability when using on-mass measurements. Regarding mass shift mode, despite peak tailing is observed at a low dwell time of 50 as well as 100 μs, the ion-burst explosion formed in these conditions due to ammonia clusters suggests no-problematic and accurate acquisition, and following explanations mentioned above similar to the Ti discussion, a dwell time of 100 μs was the best choice (Fig. S9 and S10, ESI).

Regarding ZnO NPs, the effect of the dwell time when using the mass shift approach was performed with ZnO NPs suspensions of 80–200 nm (2.5 μg L^{-1}) and recording the $^{64}Zn(NH_3)_3$ adduct at an ammonia flow rate of 1.75 mL min^{-1}; whereas, on-mass measurement (^{64}Zn) were performed with ZnO NPs suspensions of 35–45 nm(1.25 μg L^{-1}), 80–200 nm (2.5 μg L^{-1}), and <150 nm (2.5 μg L^{-1}) at an ammonia flow rate of 0.5 mL min^{-1}. Similar peak weights were observed $^{64}Zn(NH_3)_3$ adduct (mass shift approach) as shown in Fig. S11 (ESI). The study of the peak spectra when using the mass shift approach has shown that short dwell times (50 μs) are not enough for a well-defined peak registration due to poor peak intensity and low number of peaks (Table S2, ESI). Similarly, better results (peak-shape, peak intensity and number of peaks) were also obtained when using higher dwell times for mass shift monitoring (Fig. S12 and Table S2, ESI). Therefore, the recording of the $^{64}Zn(NH_3)_3$ adduct requires high dwell times, and a value of 200 μs gives the best performance in contrast to the obtained in Ti and Cu experiments. However, since the broader peaks obtained when using the mass-shift mode for Zn (Fig. S12, ESI), on-mass measurements at low ammonia flow rates are preferable for ZnO NPs, and a repeatable acquisition (good peak-shapes and high number of counted peaks) are obtained at low dwell times such as 50 μs (Fig. S11, ESI).

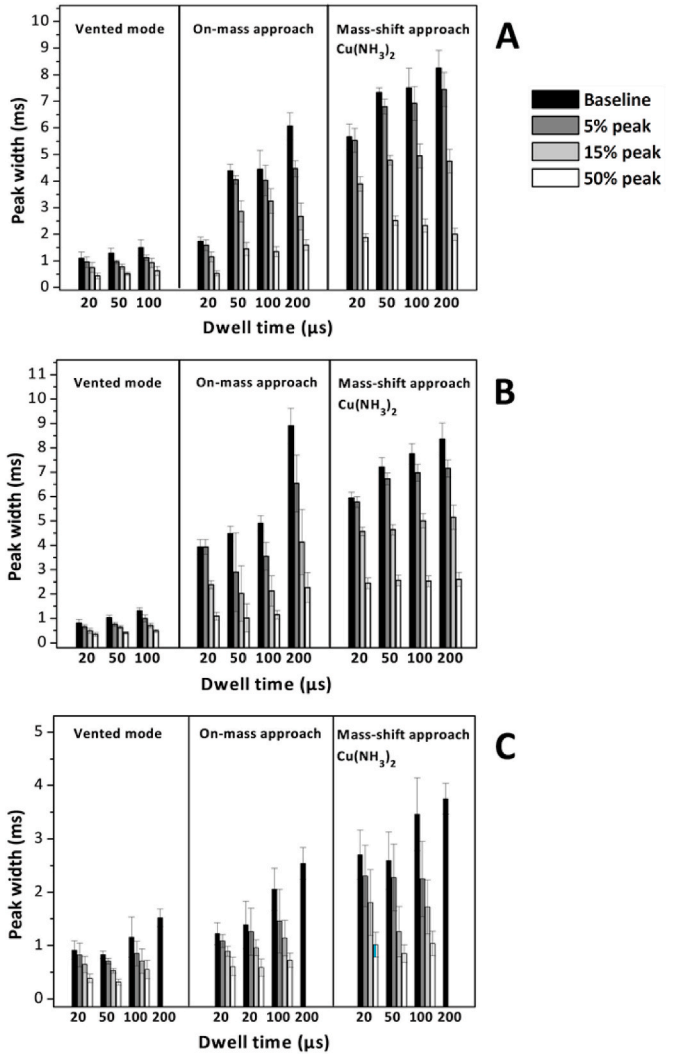

Fig. 4. Effect of the dwell time influence on peak width recorded by on-mass and mass shift approaches (ammonia flow rate of 0.5 mL min^{-1} for *m/z* 63 and 1.5 mL min^{-1} for *m/z* 97) for (A) Cu NPs of 40–60 nm, (B) Cu NPs of 60–80 nm, and (C) CuO NPs of <50 nm.

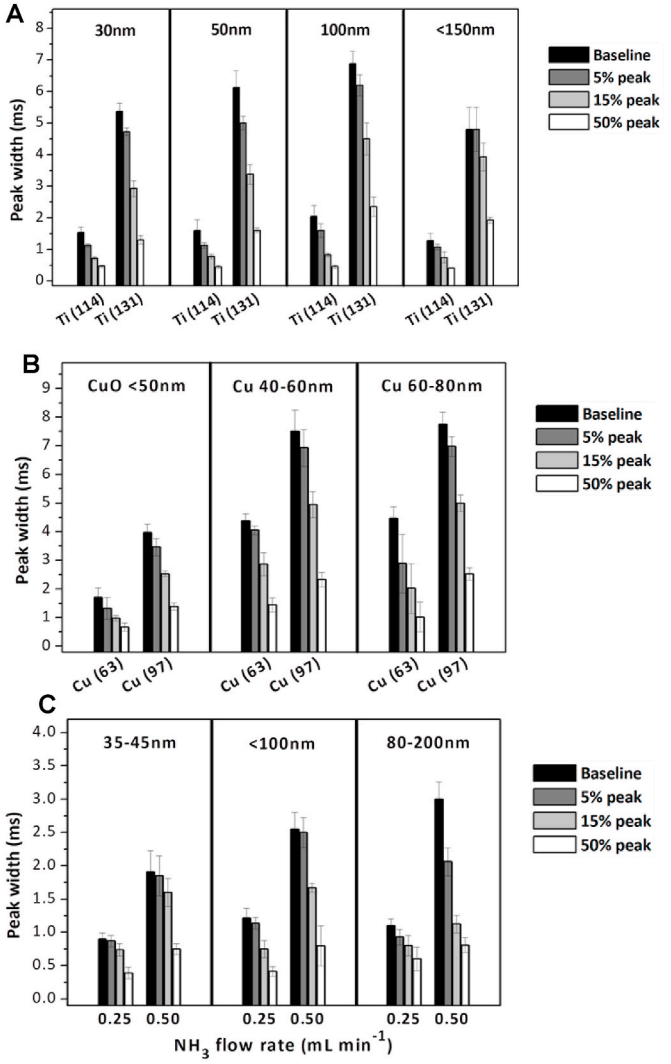

Fig. 5. Effect of the NPs size on the peak width for (A) TiO_2 NPs, (B) Cu NPs and CuO NPs, and ZnO NPs.

3.4. Influence of NP size and NP type

After fixing the ammonia flow rate and dwell time for each NP type and measurement mode (on-mass and/or mass shift), the influence of the NP size on the peak width and peak shape was investigated. The experiments were performed with suspensions of TiO_2 NPs of 30, 50 and 100 nm (1.25 µg L^{-1} of TiO_2), and <150 nm (2.5 µg L^{-1} of TiO_2); suspensions of 40–60 nm and 60–80 nm Cu NPs (2.5 µg L^{-1} of Cu), and <50 nm CuO (2.5 µg L^{-1} of CuO); and suspensions of ZnO NPs of 35–45 nm (2.5 µg L^{-1}), 80–200 nm (2.5 µg L^{-1}), and <150 nm (2.5 µg L^{-1}). Fig. 5A shows results regarding the peak width for TiO_2 NPs measurements when recording the $Ti(NH)(NH_3)_3$ (*m/z* of 114) and the $Ti(NH)(NH_3)_4$(*m/z* of 131) adducts (mass shift mode). Low influence of the TiO_2 NPs size on the peak width was observed for $Ti(NH)(NH_3)_3$ (*m/z* of 114) measurements (for instance, the baseline peak width varies between 1.5 and 2.0 ms, whereas $Ti(NH)(NH_3)_4$ (*m/z* of 131) adduct recording implies a variation between 5.0 and 7.0 ms). Similarly, the size of Cu NPs (either mass shift and on mass approaches) and the size of ZnO NPs (on-mass approach using 0.25 mL min^{-1} of ammonia) do not affect the peak width (Fig. 5B and C). However, an increase on the peak width was observed for ZnO NPs when using an ammonia flow rate of 0.5 mL min^{-1} (gradual increase from 1.9 to 3.0 ms for ZnO NPs sizes of 35–45 nm, <150 nm, and 80–200 nm, Fig. 5C). Results for on-mass measurements for ZnO NPs (ammonia flow rate of 0.5 mL min^{-1}) agree with the literature regarding SiO_2 NPs [22], and Fe_3O_4 NPs, Au NPs, Ag NPs and Pt NPs [24], for which high NPs sizes have been reported to lead broad peaks. However, results for on-mass measurements for Cu/CuO NPs, and for mass shift determinations have shown a different trend.

Finally, from Fig. 5B it can be seen that CuO NPs (size <50 nm) show narrower peaks than those measured for Cu NPs (sizes 40–60, 60–80 nm), but these findings cannot be exclusively attributed to the NP size since the composition of the NPs is different (Cu mass fraction of 79.89% for CuO NPs, and 100% for Cu NPs). The influence of the NP chemical nature is therefore important and narrower peak widths (on-mass and mass shift approaches) have been obtained for CuO NPs when comparing with Cu NPs of similar size (Fig. 5B). In addition, on mass measurements for CuO NPs show broader peak widths than ZnO NPs (Fig. 5B and C); whereas, peak widths when using the mass shift approach increase in the order of TiO_2 NPs ($^{48}Ti(NH)(NH_3)_3$) >CuO NPs ($^{63}Cu(NH_3)_2^+$) > TiO_2 NPs ($^{48}Ti(NH)(NH_3)_4$) > Cu NPs ($^{63}Cu(NH_3)_2^+$) >ZnO NPs ($^{64}Zn(NH_3)_3^+$), as shown in Fig. S13 (ESI). Ti-ammonia clusters (*m/z* 114 and 131) exhibit a well-defined peak-shape (Fig. S13, ESI) with high intensities and a high number of detected peaks (Table S1 and S2, ESI), being narrower than Cu- and Zn-ammonia clusters. As previously mentioned, Cu-ammonia clusters exhibit better

performance in their oxide nature (lower peak widths derived from CuO NPs than from Cu NPs), and broad peaks are observed for Zn-ammonia clusters (peak width close to 10 ms).

3.5. On-mass and mass shift approaches: selected conditions

On-mass measurements offer narrower peaks than those obtained when using the mass-shift mode, making it an appealing methodology mainly for assessing ZnO NPs. However, on-mass measurements were not found useful for assessing TiO_2 NPs due to the great reactivity of Ti with ammonia (and also the high-stability of Ti-ammonia clusters), which leads to a low ^{48}Ti mass abundance. Peak width related to Ti-ammonia cluster *m/z* 131 ($^{48}Ti(NH)(NH_3)_4$) is 3–4 times higher than Ti-ammonia cluster *m/z* 114 ($^{48}Ti(NH)(NH_3)_3$). This behaviour is strongly influenced by ammonia flow rate. High amounts of ammonia in the reaction cell result in a stronger ion-burst in the reaction cell. Moreover, Ti-ammonia cluster *m/z* 131 contains more molecules, resulting again in a stronger ion explosion and, consequently, a higher peak time measurement. Despite the peak width for Ti-ammonia cluster *m/z* 131($^{48}Ti(NH)(NH_3)_4$) being large (higher measurement time), the *m/z* 131 falls in a free-interference region as shown in the mass spectrum given in Fig. S14.

Cu NPs and CuO NPs can be measured by either on-mass and mass shift approaches, but, as previously mentioned, narrower peaks are obtained for on-mass measurements. The selection of one mode or other will be depend on the presence of potential interferences close to *m/z* ^{63}Cu or *m/z* $^{63}Cu(NH_3)_2^+$. However, on-mass approach leads to better results when determining ZnO NPs (0.25 mL min^{-1}).

Taking into account the peak width as well as the number of peaks and peak intensities (Table S1 and S2, ESI), selected conditions for both on-mass and mass shift modes are listed in Table 2. As previously mentioned, the ammonia flow rate required for NPs assessment is slightly lower than those required/reported for determining dissolved analytes [21], and it can be explained by the successive reaction among hundreds of atoms included in the nanoparticles. Finally, to illustrate a comparison between three different modes, Fig. S15 (Cu and CuO NPs) and Fig. S16 (ZnO NPs) were shown at their optimized conditions.

3.6. Sensitivity

The assessment of the limit of detection (LOD) and the limit of quantification (LOQ) was based on the 3 SD/m and 10 SD/m criterion, where *SD* is the standard deviation of eleven measurements of a blank; and *m* is the slope of a calibration graph. Ionic aqueous calibration for TiO_2 NPs assessment were up 2.0 μg L^{-1} (standard and mass shift mode with *m/z* 131, $^{48}Ti(NH)(NH_3)_4$) and up to 4.0 μg L^{-1} for mass shift mode with *m/z* 114, $^{48}Ti(NH)(NH_3)_3$). Similarly, ionic aqueous calibrations up to 1.0 μg L^{-1} (standard and on-mass mode, *m/z* 63) and up to 2.0 μg L^{-1} (mass shift mode with $^{63}Cu(NH_3)_2$, *m/z* 97) were performed for Cu NPs determination; whereas, calibration up to 2.0 μg L^{-1} (standard and on-mass mode, *m/z* 64) and up to 3.0 μg L^{-1} (mass shift mode with $^{64}Zn(NH_3)_3$, *m/z* 115) were used for ZnO NPs assessment. For all cases, calibration graphs were found to exhibit $r^2 > 0.999$, and the RSD% of the blank measurements were always below 7%.

The limit of detection in size (lowest size measured by SP-ICP-MS) was obtained from the Syngistix™ Nano Application software. These values (LOD in size) and the LOD/LOQ values for number concentrations are listed in Table 3. The improved sensitivity obtained for the standard mode is expected since the use of reaction/collision gases implies a reduction of sensitivity because the inherent dilution in the reaction/collision cell. Regarding DRC technology for TiO_2 NPs assessment, sensitivity is quite better when using the $^{48}Ti(NH)(NH_3)_4$ (*m/z* 131) adduct than for $^{48}Ti(NH)(NH_3)_3$ (*m/z* 114) adduct (Table 3). Mass shift measurements for Cu NPs ($^{63}Cu(NH_3)_2$, *m/z* 97) showed similar sensitivity than that obtained when working with the standard mode, but on-mass measurements were more sensitive in number concentration and size. These findings can be attributed to a proper interferences removal and a minimum dilution in the reaction cell since on–mass measurements require a low ammonia flow rate. Similar conclusions can be attained for Zn NPs, and the on-mass approach also showed the highest sensitivity (Table 3).

Table 3
Limit of detection in size and limit of detection and quantification (number concentration) for the standard mode and on-mass and mass shift approaches.

	Work-mode (*m/z*)	LOD_{size} (nm)	$LOD_{number\ concentration}$ (particles L^{-1})	$LOQ_{number\ concentration}$ (particles L^{-1})
TiO_2 NPs	STD (48)	16	2.42×10^5	8.07×10^5
	Mass-shift (114)	41	9.10×10^5	3.03×10^6
	Mass-shift (131)	23	4.51×10^5	1.50×10^6
ZnO NPs	STD (64)	19	1.06×10^6	3.53×10^6
	On-mass (64)	13	8.40×10^4	2.80×10^5
	Mass-shift (115)	31	3.58×10^6	1.19×10^7
Cu NPs	STD (63)	13	3.57×10^5	1.19×10^6
	On-mass (63)	7	3.50×10^4	1.17×10^5
	Mass-shift (97)	16	4.53×10^5	1.51×10^6

3.7. Interferences study

Titanium and Zn measurements are interfered in ICP-MS by large amounts of Ca and P, major metals present in many matrices such as biological/food materials. Therefore, the determination of 100 nm TiO_2 NPs (2.5 μg L^{-1}), 60–80 nm Cu NPs (5.0 μg L^{-1}), and 80–200 nm ZnO NPs (5.0 μg L^{-1}) under standard conditions (vented mode, no DRC technology) with the most abundant isotopes (^{63}Cu, ^{64}Zn, and ^{48}Ti), and under the optimized DRC on-mass (^{63}Cu and ^{64}Zn) and mass shift ($^{63}Cu(NH_3)_2$, *m/z* 97; $^{64}Zn(NH_3)_3$, *m/z* 115; $^{48}Ti(NH)(NH_3)_3$, *m/z* 114; and $^{48}Ti(NH)(NH_3)_4$, *m/z* 131) conditions was performed in the presence of increasing concentrations of Ca and P (up to 50 mg L^{-1} for Ti measurements and up to 10 mg L^{-1} for Cu and Zn measurements). Results in triplicate for ionic background (ionic metal concentration) and NPs concentration are given in Fig. S17. The $^{48}Ti(NH)(NH_3)_4$ (*m/z* 131) adduct was found to allow a free interference determination of TiO_2 NPs even in the presence of 10 mg L^{-1} plus 10 mg L^{-1} of Ca and P. Determinations based on monitoring the $^{64}Zn(NH_3)_3$ (*m/z* 115) adduct are not interfered up Ca plus P concentrations of 5.0 plus 5.0 mg L^{-1}: whereas, interferences were found to be important for Ca plus P concentrations of 1.0 plus 1.0 mg L^{-1} under standard conditions (Fig. S17A-B). Regarding Cu NPs, similar results were observed for on-mass (^{63}Cu) and mass shift ($^{63}Cu(NH_3)_2$, *m/z* 97) conditions, and interference free determinations were possible even in the presence of 2.0 mg L^{-1} plus 2.0 mg L^{-1} of Ca plus P (Fig. S17C-D). Calcium and P interference on Cu NPs start to be important up to 0.5 mg L^{-1} plus 0.5 mg L^{-1} of Ca plus P under the standard mode measurement (Fig. S17C-D). Finally, Fig. S16E-F shows that Ca plus P are serious interferences on the ZnO NPs assessment at 0.5 mg L^{-1} plus 0.5 mg L^{-1} of Ca plus P under the standard mode measurement and also by using the on-mass and mass shift approaches. However, on-mass measurements appear to control better the Ca plus P interference.

4. Conclusions

Conditions for DRC in ICP-MS working in single-particle mode must be carefully established because conditions, mainly reaction gas (ammonia) flow rate, are different from those required for dissolved analytes in conventional ICP-MS. Optimized conditions can be dependent on the size and the NPs type. On-mass and mass-shift approaches

have been found useful for Cu NPs and CuO NPs; whereas on-mass mode was preferred for ZnO NPs assessment. In addition, the mass shift approach is the best option for facing Ti interferences in TiO_2 NPs determinations. Regarding mass-shift mode, the recording metal-ammonia adducts generated from the second most abundant isotopes can also be appealing alternatives for overcoming complex interferences. This is the case of Cu NPs, CuO NPs and ZnO NPs because the abundance of the second most abundant isotopes (^{65}Cu and ^{66}Zn) are 31% and 28%, respectively. Finally, careful optimization has to be performed for NPs in complex samples (extracts) which can increase the background signal and can lead to other conditions for reaction gas (ammonia), flow rate and dwell time.

Credit authors statement

Cristian Suárez-Oubiña: Formal analysis, Investigation, Validation, Visualization, Writing – original draft preparation. **Paloma Herbello-Hermelo**: Data curation, Supervision, Validation. **Antonio Moreda-Piñeiro**: Software, Validation, Writing- Reviewing and Editing, Supervision, Writing- Reviewing and Editing. **Pilar Bermejo-Barrera**: Resources, Project administration, Funding acquisition.

Declaration of competing interest

The authors declare that they have no known competing financial interests or personal relationships that could have appeared to influence the work reported in this paper.

Acknowledgements

The authors wish to acknowledge the financial support of the *Ministerio de Economía y Competitividad* (INNOVANANO projects, reference RT2018-099222-B-100), and the Xunta de Galicia (*Grupo de Referencia Competitiva*, grant number ED431C2018/19).

Appendix A. Supplementary data

Supplementary data to this article can be found online at https://doi.org/10.1016/j.talanta.2022.123286.

References

[[1]] V. Sogne, F. Meier, T. Klein, C. Contado, Investigation of zinc oxide particles in cosmetic products by means of centrifugal and asymmetrical flow field-flow fractionation, J. Chromatogr., A 1515 (2017) 196–208, https://doi.org/10.1016/j.chroma.2017.07.098.

[2] J. Athinarayanan, V.S. Periasamy, M.A. Alsaif, A.A. Al-Warthan, A.A. Alshatwi, Presence of nanosilica (E551) in commercial food products: TNF-mediated oxidative stress and altered cell cycle progression in human lung fibroblast cells, Cell Biol. Toxicol. 30 (2014) 89–100, https://doi.org/10.1007/s10565-014-9271-8.

[3] A. Weir, P. Westerhoff, L. Fabricius, K. Hristovski, N. Von Goetz, Titanium dioxide nanoparticles in food and personal care products, Environ. Sci. Technol. 46 (2012) 2242–2250, https://doi.org/10.1021/es204168d.

[4] P. Van Broekhuizen, F. Van Broekhuizen, R. Cornelissen, L. Reijnders, Use of nanomaterials in the European construction industry and some occupational health aspects thereof, J. Nanoparticle Res. 13 (2011) 447–462, https://doi.org/10.1007/s11051-010-0195-9.

[5] A.M. Alkilany, L.B. Thompson, S.P. Boulos, P.N. Sisco, C.J. Murphy, Gold nanorods: their potential for photothermal therapeutics and drug delivery, tempered by the complexity of their biological interactions, Adv. Drug Deliv. Rev. 64 (2012) 190–199, https://doi.org/10.1016/j.addr.2011.03.005.

[6] B. Jovanović, G. Bezirci, A.S. Çağan, J. Coppens, E.E. Levi, Z. Oluz, E. Tuncel, H. Duran, M. Beklioğlu, Food web effects of titanium dioxide nanoparticles in an outdoor freshwater mesocosm experiment, Nanotoxicology 10 (2016) 902–912, https://doi.org/10.3109/17435390.2016.1140242.

[7] J.J. Faust, K. Doudrick, Y. Yang, P. Westerhoff, D.G. Capco, Food grade titanium dioxide disrupts intestinal brush border microvilli in vitro independent of sedimentation, Cell Biol. Toxicol. 30 (2014) 169–188, https://doi.org/10.1007/s10565-014-9278-1.

[8] European Commission, Regulation (EC) No 1223/2009 of the European parliament and of the council of 30 november 2009 on cosmetic products, Off. J. Eur. Union 22 (2009) 12 (2009) L342/59–L342/209.

[9] European commission, Regulation (EC) No 450/2009 of 29 May2009 on active and intelligent materials and articles intended to come into contact with food, Off. J. Eur. Union 30 (2009) 5, 2009) L135/3–L135/11.

[10] European Commission, Regulation (EU) No 10/2011 of 14 January 2011 on plastic materials and articles intended to come into contact with food, Off. J. Eur. Union 15 (2011) 1 (2011) L12/1–L12/89.

[11] H.E. Pace, N.J. Rogers, C. Jarolimek, V.A. Coleman, C.P. Higgins, J.F. Ranville, Determining transport efficiency for the purpose of counting and sizing nanoparticles via single particle inductively coupled plasma mass spectrometry, Anal. Chem. 83 (2011) 9361–9369.

[12] F. Laborda, E. Bolea, J. Jiménez-Lamana, Single particle inductively coupled plasma mass spectrometry: a powerful tool for nanoanalysis, Anal. Chem. 86 (2014) 2270–2278, https://doi.org/10.1021/ac402980q.

[13] F. Laborda, E. Bolea, J. Jiménez-Lamana, Single particle inductively coupled plasma mass spectrometry for the analysis of inorganic engineered nanoparticles in environmental samples, Trends Environ. Anal. Chem. 9 (2016) 15–23, https://doi.org/10.1016/j.teac.2016.02.001.

[14] M.D. Montaño, J.W. Olesik, A.G. Barber, K. Challis, J.F. Ranville, Single Particle ICP-MS: advances toward routine analysis of nanomaterials, Anal. Bioanal. Chem. 408 (2016) 5053–5074, https://doi.org/10.1007/s00216-016-9676-8.

[15] D. Mozhayeva, C. Engelhard, A critical review of single particle inductively coupled plasma mass spectrometry-A step towards an ideal method for nanomaterial characterization, J. Anal. At. Spectrom. 35 (2020) 1740–1783, https://doi.org/10.1039/c9ja00206e.

[16] N. Jakubowski, L. Moens, F. Vanhaecke, Sector field mass spectrometers in ICP-MS, Spectrochim. Acta Part B At. Spectrosc. 53 (1998) 1739–1763, https://doi.org/10.1016/S0584-8547(98)00222-5.

[17] N. Jakubowski, T. Prohaska, L. Rottmann, F. Vanhaecke, Inductively coupled plasma- and glow discharge plasma-sector field mass spectrometry: Part I. Tutorial: fundamentals and instrumentation, J. Anal. At. Spectrom. 26 (2011) 693–726, https://doi.org/10.1039/c0ja00161a.

[18] I. Rodushkin, E. Engström, A. Stenberg, D.C. Baxter, Determination of low-abundance elements at ultra-trace levels in urine and serum by inductively coupled plasma-sector field mass spectrometry, Anal. Bioanal. Chem. 380 (2004) 247–257, https://doi.org/10.1007/s00216-004-2742-7.

[19] J.M. Harrington, D.J. Young, A.S. Essader, S.J. Sumner, K.E. Levine, Analysis of human serum and whole blood for mineral content by ICP-MS and ICP-OES: development of a mineralomics method, Biol. Trace Elem. Res. 160 (2014) 132–142, https://doi.org/10.1007/s12011-014-0033-5.

[20] K. Sakata, K. Kawabata, Reduction of fundamental polyatomic ions in inductively coupled plasma mass spectrometry, Spectrochim. Acta Part B At. Spectrosc. 49 (1994) 1027–1038, https://doi.org/10.1016/0584-8547(94)80088-X.

[21] C. Suárez-Oubiña, P. Herbello-Hermelo, P. Bermejo-Barrera, A. Moreda-Piñeiro, Exploiting dynamic reaction cell technology for removal of spectral interferences in the assessment of Ag, Cu, Ti, and Zn by inductively coupled plasma mass spectrometry, Spectrochim. Acta B. 187 (2022) 106330, https://doi.org/10.1016/j.sab.2021.106330.

[22] E. Bolea-Fernandez, D. Leite, A. Rua-Ibarz, L. Balcaen, M. Aramendía, M. Resano, F. Vanhaecke, Characterization of SiO_2 nanoparticles by single particle-inductively coupled plasma-tandem mass spectrometry (SP-ICP-MS/MS), J. Anal. At. Spectrom. 32 (2017) 2140–2152, https://doi.org/10.1039/c7ja00138j.

[23] S. Candás-Zapico, D.J. Kutscher, M. Montes-Bayón, J. Bettmer, Single particle analysis of TiO_2 in candy products using triple quadrupole ICP-MS, Talanta 180 (2018) 309–315, https://doi.org/10.1016/j.talanta.2017.12.041.

[24] E. Bolea-Fernandez, D. Leite, A. Rua-Ibarz, T. Liu, G. Woods, M. Aramendia, M. Resano, F. Vanhaecke, On the effect of using collision/reaction cell (CRC) technology in single-particle ICP-mass spectrometry (SP-ICP-MS), Anal. Chim. Acta 1077 (2019) 95–106, https://doi.org/10.1016/j.aca.2019.05.077.

[25] M. Tharaud, A.P. Gondikas, M.F. Benedetti, F. Von Der Kammer, T. Hofmann, G. Cornelis, TiO_2 nanomaterial detection in calcium rich matrices by spICPMS. A matter of resolution and treatment, J. Anal. At. Spectrom. 32 (2017) 1400–1411, https://doi.org/10.1039/c7ja00060j.

[26] L. Balcaen, E. Bolea-Fernandez, M. Resano, F. Vanhaecke, Inductively coupled plasma - tandem mass spectrometry (ICP-MS/MS): a powerful and universal tool for the interference-free determination of (ultra)trace elements - a tutorial review, Anal. Chim. Acta 894 (2015) 7–19, https://doi.org/10.1016/j.aca.2015.08.053.

[27] E. Bolea-Fernandez, L. Balcaen, M. Resano, F. Vanhaecke, Tandem ICP-mass spectrometry for Sr isotopic analysis without prior Rb/Sr separation, J. Anal. At. Spectrom. 31 (2016) 303–310, https://doi.org/10.1039/c5ja00157a.

[28] J. Soto-Alvaredo, F. Dutschke, J. Bettmer, M. Montes-Bayón, D. Pröfrock, A. Prange, Initial results on the coupling of sedimentation field-flow fractionation (SdFFF) to inductively coupled plasma-tandem mass spectrometry (ICP-MS/MS) for the detection and characterization of TiO2 nanoparticles, J. Anal. At. Spectrom. 31 (2016) 1549–1555, https://doi.org/10.1039/c6ja00079g.

[29] Syngistix Nano Application Software Module for Single Particle ICP-MS. https://resources.perkinelmer.com/lab-solutions/resources/docs/PRD_Syngistix-Nano-Software-Module_011657_01.pdf (accessed January 18th 2022).

[30] L. Balcaen, E. Bolea-Fernandez, M. Resano, F. Vanhaecke, Accurate determination of ultra-trace levels of Ti in blood serum using ICP-MS/MS, Anal. Chim. Acta 809 (2014) 1–8, https://doi.org/10.1016/j.aca.2013.10.017.

[31] L. Fu, S.Y. Shi, J.C. Ma, Accurate Determination of harmful and doping elements in soft magnetic ferrite powders using inductively coupled plasma tandem mass spectrometry, Chin. J. Anal. Chem. 47 (2019) 1382–1389, https://doi.org/10.1016/S1872-2040(19)61189-8 [31] E.

[32] L. Fu, S. Shi, X. Chen, H. Xie, Analysis of impurity elements in high purity cobalt powder by inductively coupled plasma tandem mass spectrometry, Microchem. J. 139 (2018) 236–241, https://doi.org/10.1016/j.microc.2018.03.002.
[33] E. Soriano, V. Yusà, A. Pastor, M. de la Guardia, Dynamic reaction cell inductively couple plasma-mass spectrometry optimization for seawater analysis, Microchem. J. 137 (2018) 363–370, https://doi.org/10.1016/j.microc.2017.11.015.
[34] Y. Cao, J. Feng, L. Tang, C. Yu, G. Mo, B. Deng, A highly efficient introduction system for single cell- ICP-MS and its application to detection of copper in single human red blood cells, Talanta 206 (2020) 120174, https://doi.org/10.1016/j.talanta.2019.120174.
[35] B.L. Batista, J.L. Rodrigues, J.A. Nunes, V.C. de Oliveira Souza, F. Barbosa, Exploiting dynamic reaction cell inductively coupled plasma mass spectrometry (DRC-ICP-MS) for sequential determination of trace elements in blood using a dilute-and-shoot procedure, Anal. Chim. Acta 639 (2009) 13–18, https://doi.org/10.1016/j.aca.2009.03.016.
[36] B. Meermann, V. Nischwitz, ICP-MS for the analysis at the nanoscale-a tutorial review, J. Anal. At. Spectrom. 33 (2018) 1432–1468, https://doi.org/10.1039/c8ja00037a.
[37] A. Rua-Ibarz, E. Bolea-Fernandez, G. Pozo, X. Dominguez-Benetton, F. Vanhaecke, K. Tirez, Characterization of iron oxide nanoparticles by means of single-particle ICP-mass spectrometry (SP-ICP-MS)-chemical: versus physical resolution to overcome spectral overlap, J. Anal. At. Spectrom. 35 (2020) 2023–2032, https://doi.org/10.1039/d0ja00183j.